

MECHANISM OF CEREBRAL EDEMA IN CHILDREN WITH DIABETIC KETOACIDOSIS

NICOLE S. GLASER, MD, SANDRA L. WOOTTON-GORGES, MD, JAMES P. MARCIN, MD, MPH, MICHAEL H. BUONOCORE, MD, PHD, JOSEPH DICARLO, MD, E. KIRK NEELY, MD, PATRICK BARNES, MD, JENNY BOTTOMLY, BS, AND NATHAN KUPPERMANN, MD, MPH

Objectives Cerebral edema during diabetic ketoacidosis (DKA) has been attributed to osmotic cellular swelling during treatment. We evaluated cerebral water distribution and cerebral perfusion during DKA treatment in children.

Study design We imaged 14 children during DKA treatment and after recovery, using both diffusion and perfusion weighted magnetic resonance imaging (MRI). We assessed the apparent diffusion coefficients (ADCs) and measures reflecting cerebral perfusion.

Results The ADC was significantly elevated during DKA treatment (indicating increased water diffusion) in all regions except the occipital gray matter. Mean reductions in the ADC from initial to postrecovery MRI were: basal ganglia $4.7 \pm 2.5 \times 10^{-5} \text{ mm}^2/\text{s}$ ($P = .002$), thalamus $3.7 \pm 2.8 \times 10^{-5} \text{ mm}^2/\text{s}$, ($P = .002$), periaqueductal gray matter $4.3 \pm 5.1 \times 10^{-5} \text{ mm}^2/\text{s}$ ($P = .03$), and frontal white matter $2.0 \pm 3.1 \times 10^{-5} \text{ mm}^2/\text{s}$ ($P = .03$). In contrast, the ADC in the occipital gray matter increased significantly from the initial to postrecovery MRI (mean increase $3.9 \pm 3.9 \times 10^{-5} \text{ mm}^2/\text{s}$, $P = .004$). Perfusion MRI during DKA treatment revealed significantly shorter mean transit times (MTTs) and higher peak tracer concentrations, possibly indicating increased cerebral blood flow (CBF).

Conclusions Elevated ADC values during DKA treatment suggests a vasogenic process as the predominant mechanism of edema formation rather than osmotic cellular swelling. (*J Pediatr* 2004;145:164-71)

Cerebral edema is the most frequent and serious complication of diabetic ketoacidosis (DKA) in children. Clinically apparent cerebral edema occurs in approximately 1% of childhood DKA and is associated with high mortality and neurological morbidity.^{1,2} The pathogenesis of the cerebral edema, however, is not understood; investigators have attributed it to cellular swelling as a result of rapid osmolar changes occurring during intravenous infusions.³⁻⁵ Several studies, however, have shown no relationship to the volume or sodium content of the infusion nor any association with the rate of change in serum glucose concentration.^{2,6-8} This suggests that other factors may be important in the pathophysiology of DKA-related cerebral edema.

Several investigators have suggested that asymptomatic, or subclinical, cerebral edema occurs commonly, if not invariably, in pediatric DKA^{9,10} and may be present before the initiation of DKA therapy.⁹ These findings, however, have been challenged by another study and thus remain controversial.¹¹

Diffusion and perfusion magnetic resonance imaging (MRI) are advanced techniques with high sensitivity for edema and capillary blood flow, respectively. Diffusion MRI, quantified as the apparent diffusion coefficient (ADC), measures the degree of mobility of water protons in tissues.¹² The precise mechanisms by which ADC changes occur in various disease states is not completely understood. It is generally accepted, however, that conditions that expand the extracellular space (eg, vasogenic edema) are characterized by increased ADC, whereas conditions that result in cellular swelling (eg, hypoxic/ischemic injury or

See editorial, p 149.

From the Departments of Pediatrics and Radiology, and Department of Internal Medicine, Division of Emergency Medicine, University of California, Davis School of Medicine, Sacramento; and Departments of Pediatrics and Radiology, Stanford University School of Medicine, Stanford, California.

Supported by research awards from the American Diabetes Association and the University of California, Davis Health System.

Submitted for publication Oct 29, 2003; last revision received Jan 29, 2004; accepted Mar 17, 2004.

Reprint requests: Nicole Glaser, MD, Department of Pediatrics, University of California Davis, School of Medicine, 2516 Stockton Blvd, Sacramento, CA 95817. E-mail: nsglaser@ucdavis.edu.

0022-3476/\$ - see front matter

Copyright © 2004 Elsevier Inc. All rights reserved.

10.1016/j.jpeds.2004.03.045

ADC	Apparent diffusion coefficient	GCS	Glasgow Coma Scale
CBF	Cerebral blood flow	Gd	Gadolinium-DTPA
CBV	Cerebral blood volume	MRI	Magnetic resonance imaging
DKA	Diabetic ketoacidosis	MTT	Mean transit time
EPI	Echo planar imaging	TTP	Time to peak

osmotic swelling) result in a decrease in ADC.^{13,14} Perfusion MRI complements diffusion imaging. The dynamic monitoring of the first pass of an intravenously administered contrast agent can be used to assess relative cerebral blood flow (CBF) and cerebral blood volume (CBV).¹⁵⁻¹⁸

The purpose of this study was to investigate the pathophysiology of DKA-related cerebral edema through the use of diffusion and perfusion MRI. If cerebral edema during treatment were caused by osmotic shifts resulting in cellular swelling, we would anticipate that the ADC during DKA treatment would be decreased,^{14,19} and cerebral perfusion would be diminished or unchanged.

PATIENTS AND METHODS

Patient Population

Patients were eligible for participation if they were younger than 18 years, diagnosed with type I diabetes mellitus, and had DKA (defined as serum glucose >300 mg/dL, venous pH <7.25 and/or serum bicarbonate <15 mEq/L, and a positive test for urine ketones or serum ketones >3 mmol/L).

Treatment Protocol

The study was approved by the institutional review boards of the participating institutions. After obtaining written informed consent from parents or guardians, we treated enrolled patients according to a standardized DKA protocol. All patients received an initial infusion of 10 to 20 mL per kg of 0.9% saline, depending on the assessed degree of hypovolemia. Patients with persistently poor perfusion or hemodynamic instability after the initial fluid infusion were given additional infusions of 0.9% saline until normal perfusion and hemodynamic stability were established. Subsequent intravenous fluids were administered as 0.67% saline (112 mEq sodium/L) with the rate calculated to replace an estimated deficit of 70 mL/kg over 48 hours. Insulin was administered via continuous intravenous infusion at an initial rate of 0.1 U/kg/hour. Patients did not receive an initial intravenous bolus of insulin, nor were any patients treated with bicarbonate. Potassium replacement was initiated with 20 mEq potassium chloride and 20 mEq potassium phosphate per liter of intravenous fluids and was adjusted to maintain normal serum potassium concentrations. Glucose was added to the intravenous fluids when the serum glucose concentration was < 300 mg/dL. Neurological status was assessed using an age-appropriate Glasgow Coma Scale (GCS)²⁰ hourly for all patients, and every 30 minutes for patients with headache or altered mental status. For patients referred from outside hospitals, the treatment protocol was changed to that described earlier on arrival to the pediatric intensive care unit.

Imaging Procedures

Patients enrolled in the study underwent MRI including fluid attenuated inversion recovery, and diffusion and perfusion imaging at two time points: (1) during treatment for DKA (2-10 hours after the initiation of therapy), and (2)

after recovery from DKA (72 hours or more after the initiation of treatment). Images were obtained using a 1.5 Tesla Horizon EchoSpeed LX 8.3.5 imaging system (General Electric Medical Systems, Milwaukee, Wis) and a standard quadrature head coil. A three-plane localizer was performed acquiring T1 images in 5 slice locations for each orthogonal direction (repetition time [TR] 40 ms/echo time [TE] 1.5 ms, 7-mm thick sections), followed by a T2 fluid attenuated inversion recovery sequence (TR 10,000 ms/TE 147 ms/inversion recovery 2200 ms, 4.2-mm thick sections).

DIFFUSION MRI. Diffusion imaging was performed using a modified single-shot spin-echo echo planar imaging (EPI) sequence. Axial images were acquired at 19 slice locations with TR 8000 ms/TE 90.4 ms, and 5-mm thick sections. The b-value in each of the 26 diffusion gradient combinations used in the sequence was 900 s/mm². Using a custom program (TensorCalc, Maj Hedehus, Stanford University, 2000), raw diffusion images were converted to diagnostically relevant b = 0 trace, ADC (mean diffusivity), isotropic diffusion weighted imaging, fractional anisotropy, Coherence Index Anisotropy²¹ and Lattice Index Anisotropy²² image types.

We determined the ADC in five regions of interest: basal ganglia, thalamus, periaqueductal gray matter, frontal white matter, and occipital gray matter. For all regions except the periaqueductal gray matter, we measured the ADC on both the right and left sides of the brain to determine the mean ADC. A single measurement was recorded for periaqueductal gray matter.

PERFUSION MRI. A first-pass, gadolinium-enhanced technique was employed using single-shot gradient echo EPI (TR 3000/TE 40 ms, slice thickness 4.2 mm, slice gap 0.8mm). Axial images were acquired at the same 19 slice locations as for the diffusion sequence. We acquired a time-series of 26 images at each slice location with a temporal resolution set at TR 3 seconds. An automatic intravenous injector (Spectris, MedRad, Inc, Bedford, Mass) was used to administer Gadolinium-DTPA ([Gd] 0.2mL/kg; Omniscan, Amersham Health, Princeton, NJ) over 6 seconds and saline flush over 30 seconds. The dynamic EPI sequence commenced 9 seconds before the injection of contrast to insure measurement of a baseline signal level. Slice locations were acquired in a superior to inferior direction to minimize the risk that arterial blood entering each slice had been previously excited and hence partially saturated during acquisition of inferior slices.

The time-series of EPI images was analyzed using published methods.^{15,18} These methods provided estimates of regional CBV, regional mean transit time (MTT), and regional time to peak (TTP). The logarithm of the signal intensity values were taken to convert the MR image intensity to new values $C(t)$ linearly proportional to the Gd concentration according to: $C(t) = (k/TE)\log(S_0(t)/S(t))$ where $C(t)$ = Gd concentration at time t , $S_0(t)$ = baseline MRI image intensity estimated for time t , $S(t)$ = actual MRI image intensity measured at time t . TE is the effective echo time of the EPI sequence, and k is the scale factor related to the

Table. Clinical and biochemical features of children with diabetic ketoacidosis at presentation and at the time of MRI

Patient No.	Time of MRI (h)	Age (y)	Sex	Known DM	Initial glucose, mmol/L (mg/dL)	Glucose at time of MRI mmol/L (mg/dL)	Initial sodium (mmol/L)	Sodium at time of MRI (mmol/L)	Initial TCO ₂ (mmol/L)
1	2	3.5	F	N	42.1 (758)	32.2 (580)	127	123	9
2	4	9.7	M	N	34.2 (617)	19.1 (344)	135	133	9
3	4	11.9	F	N	52.5 (946)	23.7 (428)	123	135	14
4	3	15.6	M	Y	19.4 (350)	15.1 (272)	128	130	9
5	4	13.3	M	Y	32.9 (593)	15.9 (287)	136	137	4
6	4	12.7	M	N	41.4 (747)	32.0 (577)	130	134	7
7	5	15.4	F	Y	33.2 (598)	14.3 (257)	132	136	12
8	5	15.5	M	N	23.8 (429)	9.8 (177)	132	136	7
9	5	8.3	M	N	36.0 (648)	20.1 (362)	138	135	5
10	5	13.9	F	Y	66.2 (1193)	21.5 (388)	134	150	5
11	9	14.7	F	Y	39.0 (703)	15.5 (279)	134	137	13
12	10	11.5	M	N	34.7 (625)	15.6 (281)	138	141	6
13	7	12.8	F	N	45.5 (820)	13.1 (236)	130	140	10
14	9	12.1	F	Y	35.1 (632)	17.6 (317)	133	133	5
Mean	—	12.2	—	—	38.3 (689)	19.0 (341)	132	136	8
Range	2-10	3.5-15.6	—	—	19.4-66.2 (350-1193)	9.8-32.2 (177-580)	123-138	123-150	4-14

local Gd relaxivity. The $S_0(t)$ baseline MRI values were found by linear interpolation across the points of the contrast passage. To represent the precontrast baseline value, the mean value obtained from the four images before injection, and three to four images after the injection but before arrival of contrast media into the tissue, were used. To represent the postcontrast baseline value, the mean of six to eight images after bolus passage were used. Linear interpolation across the time points of contrast passage provided a model for an estimate of the increasing amount of recirculating blood during the contrast passage. The postcontrast baseline was included in the determination of the signal baseline because it represents the changed baseline level of signal from contrast recirculation.

Estimates of MTT and TTP were determined by curve fitting $C(t)$ to a gamma variant function²³ extending from the last image in the pre-contrast baseline group to the first image in the postcontrast baseline group. MTT was defined by the normalized first moment of the concentration curve $MTT = \int tC(t)dt / \int C(t)dt$. Using the gamma variant function, the integrals were solved analytically, and the MTT was written in closed form based on the parameters of the gamma variant function.

The TTP was defined as the time interval between the injection of contrast and the point in time when the maximal drop in MRI image intensity occurred. The TTP was derived by adding the time associated with the acquisition of all images considered to be part of the pre-contrast baseline, plus the time

from the last pre-contrast image to the time of the peak of the gamma-variant function fit.

The regional CBV was defined as the ratio of the integrals of the contrast curves at the tissue and a feeding artery, as given by²⁴ $CBV = (k_H/\rho)(\int C(t)dt / \int AIF(t)dt)$ where $AIF(t)$ is the arterial input function representing the Gd concentration curve at time t in the feeding artery, and $C(t)$ is the Gd concentration in the tissue at time t . Also, k_H is defined as $k_H = (1 - H_{LV}/1 - H_{SV})$, where H_{LV} and H_{SV} are the assumed hematocrit in the large vessel ($H_{LV} = 0.45$) and in the capillaries ($H_{SV} = 0.25$) of tissue volume used in $C(t)$ measurement, and ρ is defined as the tissue density (assumed 1.04 g/mL).

The gamma variant function used in this study has the usual form given by: $G(t) = K(t - t_0)^\alpha e^{-\beta(t-t_0)}$ for $t_0 \leq t < \infty$, $G(t)=0$ for $t \leq t_0$. The parameters K , α and β are determined by fitting this function to the concentration estimates derived from the experimental data, and MTT, TTP, and Peak values are determined from these estimated parameters as follows:

$$MTT = t_0 + (\alpha + 1)/\beta$$

$$TTP = t_0 + \alpha/\beta$$

$$Peak = K(\alpha/\beta)^\alpha e^{-(\alpha+1)}$$

Funtool (Research software source code, GE Medical Systems, Waukesha, Wis, 1999) was used for the calculation

TCO ₂ at time of MRI (mmol/L)	Initial serum urea nitrogen, mmol/L (mg/dL)	Serum urea nitrogen at time of MRI (mg/dL)	Initial creatinine, μmol/L (mg/dL)	Creatinine at time of MRI, μmol/L (mg/dL)	Initial pH (venous)	pH at time of MRI (venous)	Initial pCO ₂ (mm Hg)	pCO ₂ at time of MRI (mm Hg)
7	8.6 (24)	7.1 (20)	76 (1.0)	69 (0.9)	7.17	7.16	25	19
11	8.2 (23)	6.8 (19)	114 (1.5)	76 (1.0)	7.12	7.19	10	25
10	4.6 (13)	2.9 (8)	84 (1.1)	61 (0.8)	—	7.28	—	24
8	5.4 (15)	5.0 (14)	99 (1.3)	91 (1.2)	—	7.16	—	22
6	8.6 (24)	7.1 (20)	99 (1.3)	91 (1.2)	7.21	7.14	24	25
5	6.4 (18)	6.1 (17)	114 (1.5)	91 (1.2)	6.99	7.01	23	19
10	6.1 (17)	3.6 (10)	91 (1.2)	69 (0.9)	7.18	7.25	36	11
9	6.8 (19)	5.7 (16)	130 (1.7)	107 (1.4)	6.98	7.12	29	25
10	5.4 (15)	4.6 (13)	76 (1.0)	61 (0.8)	7.18	7.17	12	29
11	7.8 (22)	6.4 (18)	183 (2.4)	122 (1.6)	7.07	7.29	10	27
11	9.3 (26)	7.8 (22)	114 (1.5)	91 (1.2)	7.15	7.19	32	31
17	7.1 (20)	4.6 (13)	69 (0.9)	61 (0.8)	7.10	7.30	7	31
13	7.8 (22)	4.6 (13)	107 (1.4)	61 (0.8)	7.13	7.22	14	39
7	16.4 (46)	13.9 (39)	160 (2.1)	99 (1.3)	7.10	7.13	19	22
10	7.7 (22)	6.2 (17)	108 (1.4)	82 (1.1)	7.11	7.19	20	25
5-17	4.6-16.4 (13-46)	2.9-13.9 (8-39)	69-183 (0.9-2.4)	61-122 (0.8-1.6)	6.98-7.21	7.01-7.30	7-36	11-39

of $S_0(t)$, $S(t)$, $C(t)$, the least squares fit of the concentration estimates to the gamma variant function, and determination of peak tracer concentration, MTT, TPP, and CBV, according to the equations here. Calculation of CBF based on the calculation of a Residue Function for each voxel,^{16,17} was not performed because software for the analysis was not available.

We avoided pharmacological sedation during the imaging procedures whenever possible. When necessary, sodium pentobarbital (2 mg/kg or less) or midazolam (0.1 mg/kg or less) were used.

Statistical Analysis

We compared ADC values and hemodynamic measures during DKA treatment to those measured after recovery using the Wilcoxon signed rank test.

RESULTS

We enrolled 14 children with DKA into the study (Table). At enrollment, 6 children complained of headache, and 1 child had substantially altered mental status with a GCS score of 6. This child's mental status improved after 5 hours of treatment for DKA and returned to normal after 12 hours. Five additional children had deteriorations in mental status (decline in GCS score below 15) during treatment. Four of these declines were mild (minimum GCS score of 14). The fifth child had a decline in GCS score to 11 at hour 7 but

returned to normal by hour 10. None of these children were treated for cerebral edema because their MR inversion recovery imaging sequences did not demonstrate overt evidence of cerebral swelling (ie, reduced ventricular size, inapparent basilar cisterns, or intensity abnormalities). All patients recovered fully and without neurologic deficit. All patients maintained normal age-adjusted blood pressures throughout the study. Three children received pharmacological sedation for their initial imaging studies, and 1 child received sedation for the follow-up imaging study.

In four of the five cerebral anatomical regions evaluated, ADC values were significantly elevated during DKA treatment in comparison with values measured after recovery. These findings suggest a predominance of extracellular over intracellular fluid accumulation, most consistent with vasogenic edema (Fig 1). In contrast, significantly lower ADC values were observed in the occipital gray matter during DKA treatment compared with values measured after recovery, indicating that water distribution in this area of the brain during DKA treatment differs from the other anatomical regions.

On perfusion MRI, we found that the MTT was significantly shorter during DKA treatment than after recovery in all regions of interest (Fig 2). The TTP tracer concentration tended to be shorter during DKA treatment as well, but these differences did not achieve statistical significance (P values .07-.14). The peak tracer concentration was significantly

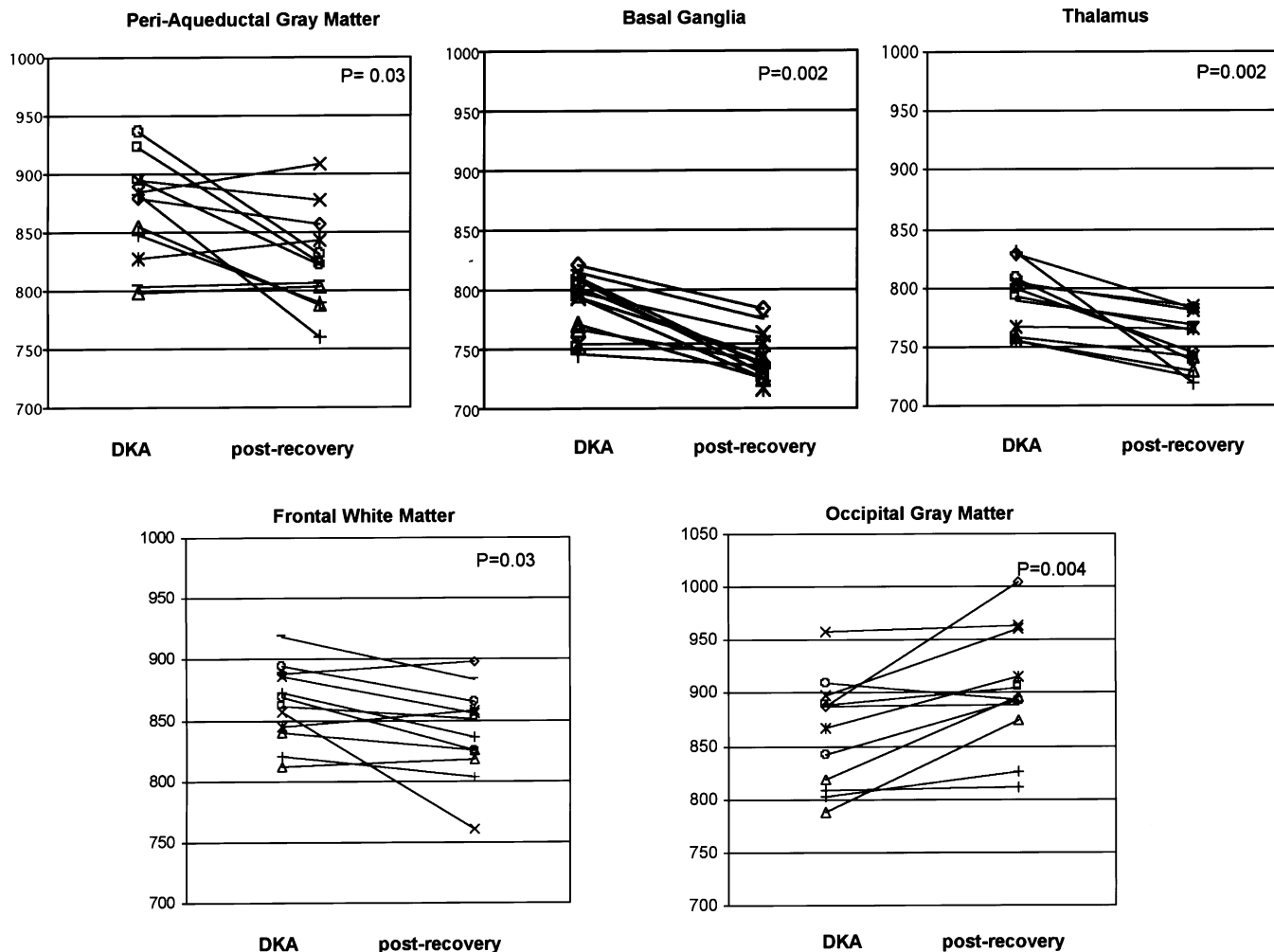


Fig 1. ADC values ($\mu\text{m}^2/\text{s}$) measured during treatment for DKA and after recovery from the DKA episode. ADC values at one or both time points were not obtained for 2 patients enrolled in the study because of technical difficulties or patient movement during imaging.

greater during DKA treatment in all anatomical regions except the occipital gray matter. CBV did not change significantly between the two examinations in any of the regions.

DISCUSSION

This study provides new information regarding cerebral edema during DKA. First, our diffusion MRI data provide further evidence that subtle, asymptomatic cerebral edema may occur commonly in children during DKA treatment^{9,10} because we consistently observed changes in ADC on diffusion MRI, although most patients had no symptoms or signs of cerebral edema. More important, however, our findings demonstrate that the ADC is increased, rather than decreased, during DKA treatment in most regions of the brain, likely indicating expansion of the extracellular space relative to the intracellular space.¹² These findings are most consistent with a vasogenic mechanism of edema formation rather than osmotic cell swelling, which is associated with expansion of the intracellular space.^{14,19} In studies of cerebral edema caused by osmotic cell swelling, a decrease in ADC has been observed.^{14,19}

Our perfusion MRI data consistently demonstrate decreased MTT and increased peak tracer concentration on the initial scans. These changes are consistent with increased cerebral perfusion during DKA treatment,^{25,26} however, we cannot exclude the possibility that the observed changes may, at least in part, reflect differences in the patients' hemodynamic states between the two scans rather than changes in cerebral perfusion. Few studies have evaluated the impact of systemic volume depletion or expansion on perfusion imaging. Existing studies suggest that severe volume depletion may increase MTT and volume expansion with increased blood pressure may decrease TTP.^{27,28} These studies lend support to the hypothesis that the observed findings were a result of changes in cerebral perfusion; however, the impact of less severe volume depletion, similar to that which occurs in DKA, on perfusion imaging has not been investigated.

A number of possible mechanisms might contribute to vasogenic cerebral edema in DKA. Some investigators have proposed that ketone bodies may act directly on the brain microvascular endothelium to cause vasogenic edema.^{29,30} Beta-hydroxybutyrate and acetoacetate may stimulate production of vasoactive peptides by cultured brain endothelial

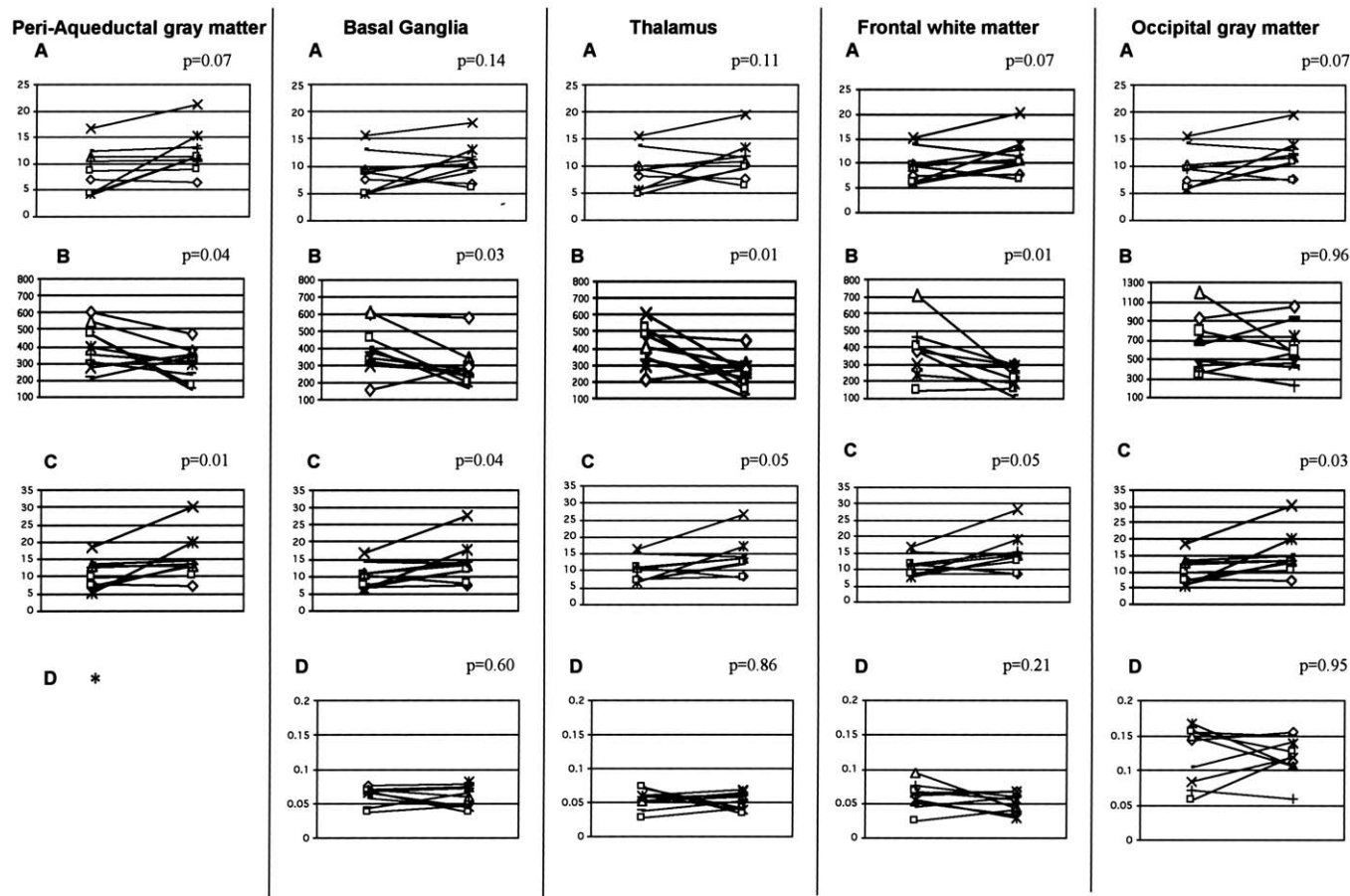


Fig 2. Perfusion MRI measures in children with DKA during treatment and after recovery from the DKA episode. **A**, TTP tracer concentration (s); **B**, Maximum tracer concentration; **C**, MTT (s); **D**, CBV (mL/g of tissue). *CBV was not measured in the periaqueductal gray matter because of inaccuracies of this measure in regions with high cerebrospinal fluid content. Perfusion MRI measurements at one or both time points were not obtained for 5 patients enrolled in the study because of either technical difficulties or patient movement during imaging (3 patients) or because of lack of consent for administration of intravenous contrast (2 patients).

cells, and these peptides may increase vascular permeability.³⁰ In addition, acetoacetate may increase the expression of intercellular adhesion molecule-1, promoting cerebrovascular leakage.^{29,31}

A study of risk factors for cerebral edema in childhood DKA conducted by our group showed that patients with greater dehydration and those with more profound hypocapnia are at increased risk of symptomatic cerebral edema.² These findings suggest that cerebral hypoperfusion before DKA treatment, and subsequent reperfusion, might play a role in the pathogenesis of cerebral edema. Reperfusion of ischemic cerebral tissue causes vasodilation³² and may impose vasogenic edema on existing cytotoxic edema to result in further cerebral injury,^{33,34} particularly in the setting of hyperglycemia.³⁵⁻³⁷ In children with DKA, cerebral edema may possibly be triggered by similar mechanisms when intravenous rehydration re-establishes normal perfusion in previously hypoperfused brain tissue.

Typically, ischemic brain injury is characterized in the acute to subacute phases by low ADC values (ie, restricted diffusion), likely a result of both astrocytic swelling and diminished intracellular microcirculation.^{38,39} The elevated

ADCs observed in this study, however, do not contradict a possible role for cerebral hypoperfusion in the pathogenesis of DKA-related cerebral edema. In fact, studies have demonstrated that the ADC may return to normal within 1 hour after reperfusion of ischemic tissue.³⁸ Ethical concerns prohibited us from delaying treatment in order to image patients before initiating therapy. It is therefore possible that MRI before rehydration would have demonstrated low ADC values.

Changes in PaCO₂ may also effect CBF during DKA treatment. Modulation of PaCO₂ has a linear effect on CBF, and hyperventilation is often utilized therapeutically to decrease CBV by inducing constriction of cerebral vessels. During DKA, children are often profoundly hypocapnic, and extreme hypocapnia may lead to cerebral hypoperfusion.^{40,41} When PaCO₂ rises after a period of hypocapnia, however, cerebral hyperemia may occur, increasing CBF beyond baseline levels.^{42,43} Because a similar rise in PaCO₂ occurs during DKA treatment, CBF may increase via similar mechanisms.

In the current study, we found decreased ADCs in the occipital gray matter during DKA treatment, in contrast to the

increased values observed in other regions. The reason for this variation may be related to the relatively less sympathetic innervation of the vertebrobasilar circulation, as compared with the carotid circulation and its diminished capacity for autoregulation of CBF.⁴⁴ These differences may predispose the occipital cortex to ischemic injury or to delayed recovery from ischemia. Cerebral edema caused by severe hypertension (posterior reversible encephalopathy syndrome) tends to involve the cerebral territories of the posterior circulation; this has been attributed similarly to failure of cerebral autoregulation in this region.⁴⁵

There are some limitations to the current study. First, because patients were not imaged before therapy for DKA, we cannot determine which of the observed changes occur as a result of DKA and which are treatment-related. Second, the patients in the current study had subclinical, rather than overt, symptomatic cerebral edema. We cannot be certain, therefore, that patients with overt cerebral edema would manifest similar characteristics on MRI. In addition, patients were imaged over a relatively broad time period, and this may have increased variability in the MR values measured. Symptomatic cerebral edema during DKA treatment, however, occurs most frequently 2 to 10 hours after initiation of therapy,² and this was the interval during which imaging took place. Nevertheless, had the timing of the imaging studies been more uniform relative to treatment initiation, we may have been better able to detect differences in the measured values.

In summary, our study indicates that during DKA treatment the ADC is increased, likely indicating expansion of the extracellular space in relation to the intracellular space. Cerebral perfusion may be increased as well. These observations contrast with those that would be expected if cerebral edema during DKA treatment were caused by osmotic cell swelling and suggest a vasogenic mechanism of edema formation.

We gratefully acknowledge the technical assistance of Greg Davis and John Ryan in conducting the MR protocol. We are also grateful to Michael Moseley, PhD, Martha O'Donnell, PhD, Steve Anderson, PhD, Richard Latchaw, MD, Laura Bachrach, MD, and Darrell Wilson, MD, for their assistance and advice throughout the course of the study.

REFERENCES

- Edge J, Hawkins M, Winter D, Dunger D. The risk and outcome of cerebral oedema developing during diabetic ketoacidosis. *Arch Dis Child* 2001;85:16-22.
- Glaser N, Barnett P, McCaslin I, et al. Risk factors for cerebral edema in children with diabetic ketoacidosis. *N Engl J Med* 2001;344:264-9.
- Harris G, Fiordalisi I. Physiologic management of diabetic ketoacidemia: a 5-year prospective pediatric experience in 231 episodes. *Arch Pediatr Adolesc Med* 1994;148:1046-52.
- Duck S, Wyatt D. Factors associated with brain herniation in the treatment of diabetic ketoacidosis. *J Pediatr* 1988;113:10-4.
- Bohn D, Daneman D. Diabetic ketoacidosis and cerebral edema. *Curr Opin Pediatr* 2002;14:287-91.
- Hale P, Rezvani I, Braunstein A, Lipman T, Martinez N, Garibaldi L. Factors predicting cerebral edema in young children with diabetic ketoacidosis and new onset type I diabetes. *Acta Paediatr* 1997;86:626-31.
- Mel J, Werther G. Incidence and outcome of diabetic cerebral oedema in childhood: are there predictors? *J Paediatr Child Health* 1995;31:17-20.
- Rosenbloom A. Intracerebral crises during treatment of diabetic ketoacidosis. *Diabetes Care* 1990;13:22-33.
- Hoffman W, Steinhart C, El Gammal T, Steele S, Cuadrado A, Morse P. Cranial CT in children and adolescents with diabetic ketoacidosis. *AJNR* 1988;9:733-9.
- Krane E, Rockoff M, Wallman J, Wolfsdorf J. Subclinical brain swelling in children during treatment of diabetic ketoacidosis. *N Engl J Med* 1985;312:1147-51.
- Smedman L, Escobar R, Hesser U, Persson B. Sub-clinical cerebral edema does not occur regularly during therapy for diabetic ketoacidosis. *Acta Paediatr* 1997;86:1172-6.
- Neumann-Haefelin T, Moseley M, Albers G. New magnetic resonance imaging methods for cerebrovascular disease: emerging clinical applications. *Ann Neurol* 2000;47:559-70.
- Gass A, Niendorf T, Hirsch J. Acute and chronic changes of the apparent diffusion coefficient in neurological disorders: biophysical mechanisms and possible underlying histopathology. *J Neurol Sci* 2001;186: S15-S23.
- Sevick R, Kanda F, Mintorovitch J, et al. Cytotoxic brain edema: assessment with diffusion-weighted MR imaging. *Radiology* 1992;185: 687-90.
- Rempp K, Brix G, Wenz F, Becker C, Guckel F, Lorenz W. Quantification of regional cerebral blood flow and volume with dynamic susceptibility contrast-enhanced MR imaging. *Radiology* 1994;193:637-41.
- Ostergaard L, Sorensen A, Kwong K, Weisskoff R, Gyldensted C, Rosen B. High resolution measurement of cerebral blood flow using intravascular tracer bolus passages. Part II: Experimental comparison and preliminary results. *Magn Reson Med* 1996;36:726-36.
- Ostergaard L, Weisskoff R, Chesler D, Gyldensted C, Rosen B. High resolution measurement of cerebral blood flow using intravascular tracer bolus passages, I: mathematical approach and statistical analysis. *Magn Reson Med* 1996;36:715-25.
- Rosen B, Belliveau J, Vevea J, Grady T. Perfusion imaging with NMR contrast agents. *Magn Reson Med* 1990;14:249-65.
- Vajda Z, Pedersen M, Doczi T, et al. Effects of centrally administered arginine vasopressin and atrial natriuretic peptide on the development of brain edema in hyponatremic rats. *Neurosurgery* 2001;49:697-705.
- Reilly P, Simpson D, Sprod R, Thomas L. Assessing the conscious level in infants and young children: a paediatric version of the Glasgow Coma Scale. *Child's Nerv Syst* 1988;4:30-3.
- Klingberg T, Vaidya C, Gabrieli J, Moseley M, Hedehus M. Myelination and organization of the frontal white matter in children: a diffusion tensor MRI study. *Neuroreport* 1999;10:2817-21.
- Pierpaoli C, Basser P. Toward a quantitative assessment of diffusion anisotropy. *Magn Reson Med* 1997;38:893-890.
- Thompson H, Starmer C. Indicator transit time considered as a gamma variate. *Circ Res* 1964;XIV:502-15.
- Axel L. Cerebral blood flow determination by rapid-sequence computed tomography. *Radiology* 1980;137:679-86.
- Grandin C, Duprez T, Smith A, et al. Which MR-derived perfusion parameters are the best predictors of infarct growth in hyperacute stroke? comparative study between relative and quantitative measurements. *Radiology* 2002;223:361-70.
- Singer O, de Rochemont R, Foerch C, et al. Relation between relative cerebral blood flow, relative cerebral blood volume, and mean transit time in patients with acute ischemic stroke determined by perfusion-weighted MRI. *J Cerebr Blood Flow Metab* 2003;23:605-11.
- Hillis A, Kane A, Tuffiash E, et al. Reperfusion of specific brain regions by raising blood pressure restores selective language functions in subacute stroke. *Brain and Language* 2001;79:495-510.
- Ishikawa S, Yokoyama K, Kuroiwa T, Makita K. Apparent diffusion coefficient mapping predicts mortality and outcome in rats with intracerebral haemodynamic disturbance: potential role of intraoperative diffusion and perfusion weighted magnetic resonance imaging to detect cerebral ischaemia. *Br J Anaesth* 2002;89:605-13.

29. Hoffman W, Cheng C, Passmore G, Carroll J, Hess D. Acetoacetate increases expression of intracellular adhesions molecule-1 (ICAM-1) in human brain microvascular endothelial cells. *Neuroscience Letters* 2002;334:71-4.
30. Isales C, Min L, Hoffman W. Acetoacetate and B-hydroxybutyrate differentially regulate endothelin-1 and vascular endothelial growth factor in mouse brain microvascular endothelial cells. *J Diab Comp* 1999;13:91-7.
31. Stanimirovic D, Wong J, Shapiro A, Durkin J. Increase in surface expression of ICAM-1, VCAM-1 and E-selectin in human cerebrovascular endothelial cells subjected to ischemia-like insults. *Acta Neurochir* 1997;70(suppl):12-6.
32. Marchal G, Young A, Baron J. Early postischemic hyperperfusion: pathophysiologic insights from positron emission tomography. *J Cereb Blood Flow Metab* 1999;19:467-82.
33. Yang G, Betz A. Reperfusion-induced injury to the blood-brain barrier after middle cerebral artery occlusion in rats. *Stroke* 1994;25:1658-64.
34. Aronowski J, Strong R, Grotta J. Reperfusion injury: demonstration of brain damage produced by reperfusion after transient focal ischemia in rats. *J Cereb Blood Flow Metab* 1997;17:1048-56.
35. Lin B, Ginsberg M, Busto R, Li L. Hyperglycemia triggers massive neutrophil deposition in brain following transient ischemia in rats. *Neuroscience Letters* 2000;278:1-4.
36. Parsons M, Barber P, Desmond P, et al. Acute hyperglycemia adversely affects stroke outcome: a magnetic resonance imaging and spectroscopy study. *Ann Neurol* 2002;52:20-8.
37. Els T, Klisch J, Orszagh M, et al. Hyperglycemia in patients with focal cerebral ischemia after intravenous thrombolysis: influence on clinical outcome and infarct size. *Cerebrovasc Dis* 2002;13:89-94.
38. Neumann-Haefelin T, Kastrup A, De Crespigny A, et al. Serial MRI after transient focal cerebral ischemia in rats: dynamics of tissue injury, blood-brain barrier damage and edema formation. *Stroke* 2000;31:1965-73.
39. Sener R. Diffusion MRI: apparent diffusion coefficient (ADC) values in the normal brain and a classification of brain disorders based on ADC values. *Comput Med Imaging Graph* 2001;25:299-326.
40. Skippen P, Seear M, Poskitt K, et al. Effect of hyperventilation on regional cerebral blood flow in head-injured children. *Crit Care Med* 1997;25:1402-9.
41. Marion D, Firlik A, McLaughlin M. Hyperventilation therapy for severe traumatic brain injury. *New Horizons* 1995;3:439-47.
42. Raichle M, Posner J, Plum F. Cerebral blood flow during and after hyperventilation. *Arch Neurol* 1970;23:394-403.
43. Gleason C, Short B, Jones M. Cerebral blood flow and metabolism during and after prolonged hypocapnia in newborn lambs. *J Pediatr* 1989;115:309-14.
44. Edvinsson L, Owman C, Sjoberg N. Autonomic nerves, mast cells, and amine receptors in human brain vessels: a histochemical and pharmacological study. *Brain Res* 1976;115:377-93.
45. Covarrubias D, Luetmer P, Campeau N. Posterior reversible encephalopathy syndrome: prognostic utility of quantitative diffusion-weighted MR images. *Am J Neuroradiol* 2002;23:1038-48.